EXPERIMENTAL STUDY OF THERMOACOUSTIC INSTABILITY IN DUCTED PREMIXED FLAMES: PERIODIC, QUASI-PERIODIC AND CHAOTIC OSCILLATIONS

Lipika Kabiraj[1], Aditya Saurabh[1], Pankaj Wahi[2], Sujith R I*[1]

[1] Department of Aerospace Engineering, Indian Institute of Technology Madras, India
[2] Department of Mechanical Engineering, Indian Institute of Technology Kanpur, India
* Corresponding author: sujith@iitm.ac.in

To study the nonlinear behavior of thermoacoustic instability, experiments were conducted on a setup comprising of laminar premixed flames confined in a duct. The observed oscillations in pressure and heat release rate during the instability were studied in the framework of dynamical systems theory. It was found that as the flame location relative to the duct was gradually varied, the oscillations underwent transitions in their qualitative behavior. Periodic, quasi-periodic and chaotic oscillations were observed at different flame locations in the duct.

Keywords : Thermoacoustic instability; Nonlinear dynamics; Quasi-periodic; Chaos

1 Introduction

Thermoacoustic instability is a plaguing problem encountered during the development of practical combustion systems such as gas turbine combustors, burners, furnaces etc. It is manifested in the form of large amplitude pressure oscillations. These oscillations induce structural vibrations which are highly detrimental to the system. Novel lean premixed combustion systems which have low NOx emission are particularly prone to thermoacoustic instability [14]. This instability occurs due to the feedback between the unsteady heat release and the acoustic oscillations in a system.

Prediction and control of thermoacoustic instabilities is indispensable for the development of new combustion technologies, and hence, is a topic of intense research worldwide. However, the problem is far from solved and is still a challenging subject. In the attempt to design effective control techniques and to identify safe operating regions, it is important to understand and characterize the nature of thermoacoustic instability. Since thermoacoustic instability is essentially a nonlinear phenomenon, a major part of this understanding is associated with the nonlinear dynamics of a thermoacoustic system. Linear methods of analyzing thermoacoustic instability are based on the study of the evolution of infinitesimally small perturbations [3] and cannot predict nonlinear phenomena such as triggering and limit cycle. Therefore, any prediction algorithm or control strategy is incomplete without the inclusion of nonlinear effects.

Recently, a lot of effort is being dedicated to explain the nonlinear behavior of thermoacoustic instabilities. A large number of investigations on nonlinearities in thermoacoustic instabilities deal with the measurement of transfer function for the heat release response of combustion systems [10, 14, 20]. Noiray *et al.* [17] have presented a rigorous investigation of thermoacoustic oscillations based on a describing function approach. Jahnke and Culick [8], through their analytical formulation of thermoacoustic instabilities in a uniform cross section combustor, had first observed quasi-periodic thermoacoustic oscillations, on consideration of higher acoustic modes. Sterling and Zukoski [21] discussed the

driving and damping mechanisms involved in the process of thermoacoustic instability through experiments on a premixed dump combustor setup. On the basis of these experiments, Sterling later [22] conducted bifurcation analysis through models assuming that the nonlinearities involved are due to combustion processes. Lei and Turan [11] pointed out the effect of vaporization processes on the nonlinear behavior of the instability.

In order to understand the underlying physics behind the occurrence of thermoacoustic instabilities and to accelerate the efforts in developing effective control strategies, careful experiments are required to investigate the nonlinear dynamics of thermoacoustic systems. The approach currently being adopted to deal with these instabilities is to avoid it by defining the safe operating regions of combustion systems in terms of its operating parameter. As a sensitive operating parameter is changed, thermoacoustic instability appear in the form of limit cycle oscillations, when the driving and damping processes in the system achieve a balance [14]. In the process of understanding the instability, a natural question that arises is whether these oscillations remain in this limit cycle behavior as the operating parameter is further changed. The current study is aimed at providing an answer to this question. In particular, the present work is based on the application of the theory of nonlinear dynamics to experimentally obtained results from a simple laboratory combustion system.

This paper gives the analysis of results obtained from experiments on a laminar premixed combustion setup using nonlinear time series analysis. It is divided into three major sections. The first section gives the details of the experimental setup and the data acquisition instruments used. This is followed by a brief discussion on selected concepts from the theory of nonlinear dynamics, which have been incorporated in the study. The next section discusses the results obtained from the experiments performed on the system with conclusions drawn in the last section.

2 Experimental Setup

A schematic of the experimental setup is shown in Fig. 1. The system essentially consists of two parts – a combustion source and a duct to confine this source. The combustion source is a premixed burner; its configuration is similar to the multiple injection configuration used by Noiray *et al* [17]. It comprises of seven small conical flames arranged symmetrically. The flames are anchored on a perforated copper block of 18 mm height which in turn is inserted in the burner tube. A fine wire mesh is mounted on the top of the burner to hold the flames from blowing off during the instability. Each hole in the block is 2 mm in diameter. A long tube of length 800 mm, inner diameter 16 mm and wall thickness 1.5 mm is chosen as the burner tube. The burner is enclosed by a 800 mm long glass duct of inner diameter 56.7 mm. An open-closed boundary condition for the acoustics in the duct is achieved by closing the bottom end of the glass tube with a metallic plate while the upper end is open to the atmosphere. The relative location of the flames in the duct can be easily changed using a traverse mechanism to move the glass duct vertically.

A premixed mixture of LPG (Liquefied Petroleum Gas) and air is introduced in the burner tube through a decoupling chamber. The chamber is shaped as a cylinder with a conical top. The cylinder has an inner diameter of 200 mm and is 200 mm in its overall height. LPG and air are mixed in a small chamber 100 mm in length and 6 mm in diameter, upstream of the decoupler. Steel wool is stuffed inside the premixing chamber to ensure proper mixing. In addition to this, the inlet of air and LPG to the chamber is made perpendicular to each other for better mixing. The experiments have been conducted for an equivalence ratio (ϕ) of 0.41 for the mixture and air flow rate of 4 lpm.

Two pressure microphones, mounted on the walls of the glass duct were used to capture the pressure oscillations at positions shown by $P1$ and $P2$ in the Fig.1. The pressure time series (p) used for the analysis in this paper were obtained from the microphone mounted near the close end of the glass duct ($P1$), at a distance of 5 cm from the bottom. This particular choice was made because the closed end will always have the maximum amplitude of pressure oscillation. The intensity fluctuations, which are proportional to the heat release rate oscillations (q) in the flame, were detected simultaneously with pressure oscillations using a photomultiplier tube equipped with a CH radical filter (431.4 nm). Data was acquired using A/D card (NI-6143) at a sampling rate of 10 kHz.

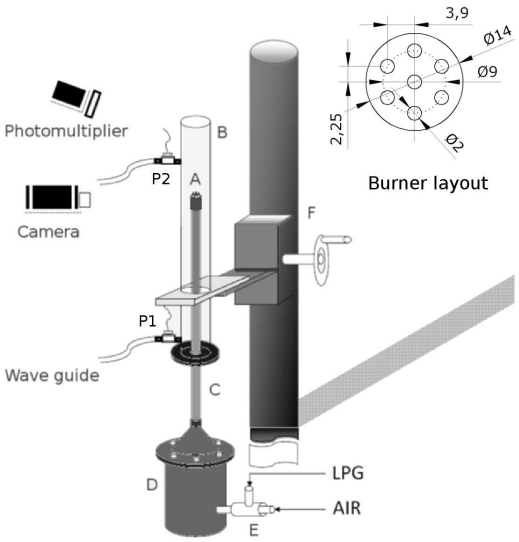

Figure 1: Schematic of the setup, A-multiple flames, B-open-closed glass duct, C-burner tube, D- decoupler, E- LPG-air premixer, F-traverse, P1, P2-pressure sensors. A top view of the burner is given at the top right corner of the figure. All dimensions are in mm.

In order to study the nature of thermoacoustic oscillations in the setup, the location of the premixed flames, initially kept at the open end is changed, gradually moving towards the closed end. All the other parameters are maintained constant, as the control parameter - the flame location (x_f) - measured from the open end of the duct, is varied. This particular method of analysis, where the qualitative change in the behavior of the system is studied as one control parameter is changed, keeping all other variables constant, is formally known as a bifurcation analysis; the control parameter (x_f in our case) is called the bifurcation parameter.

3 Bifurcation analysis

A qualitative change in the behavior exhibited by any dynamical system on changing a control parameter is termed as bifurcation. Such a change in behavior in a thermoacoustic system is seen, for instance, when the control parameter crosses the linearly stable regime. The system goes from a steady state with no oscillations to a state where we observe pressure and heat release rate oscillations. This particular type of bifurcation is called a Hopf bifurcation and the value of the parameter at which this jump occurs is termed as the Hopf point. The bifurcation plot obtained for the present system on changing the flame location is shown in Fig. 2. On the X-axis of the figure, lies the control parameter - (x_f). The Y-axis is the amplitude of pressure oscillations. The amplitudes of peaks in the pressure oscillations are obtained and plotted for each (x_f), for several cycles. For the present case about 100 cycles have been used to obtain the peak amplitudes. For a simple limit cycle oscillation, each (x_f) will have a single point corresponding to the peak amplitude of the oscillation. This can be seen in region (II) in Fig. 2. The point where region (II) starts is the Hopf point for our system. There are other regions in the plot which have more than one point. These regions are an indication that the oscillations behave differently when compared to limit cycle oscillations.

It is evident from Fig.2 that the oscillations observed in the system display both periodic and aperiodic behavior. In this paper, the oscillating behavior obtained for each value of x_f is characterized through the obtained time series data of pressure and heat release rate oscillations, using concepts from dynamical systems theory - studying phase plots and the Poincaré sections in conjunction with the time-series and its power spectrum density (equivalent to the Fast Fourier Transform). These concepts are briefly described below before discussing the nonlinear time series analysis method used for phase reconstruction.

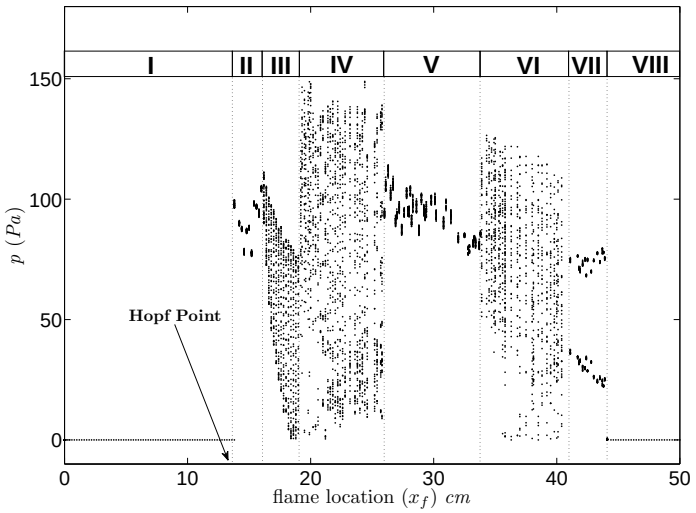

Figure 2: Bifurcation plot: Hopf point at $x_f = 13.8\ cm$, region I-steady state, region II-limit cycle oscillations, region III-quasi-periodic behavior, region IV- chaotic, region V- period-4 and frequency-locking, region VI- chaotic, region VII- period-2, region VIII-steady state.

3.1 Phase orbits or trajectories or phase portraits

The phase space of a dynamical system consists of the independent state variables which completely specify the state of the system at any given time. A knowledge of these state variables allows us to evolve the system forward in time in a unique manner. In this phase space, all possible states of the system are represented by points. The curve joining the set of points in the state space which result from an evolution in time gives a phase orbit or trajectory. Such orbits help in the diagnosis of an attractor (the limit set approached after long time) as a limit cycle, a quasi-periodic solution or a chaotic solution. For a limit cycle, the attractor is a closed curve in the phase space, indicating that the solution is periodic in nature. A quasi-periodic solution consists of two independent incommensurate frequencies and as a result the time evolution shows modulations in the amplitudes of the solutions. The corresponding phase trajectories of the attractor fill a torus in the phase space. For chaotic solutions, there is an almost continuous spectrum of frequencies (broadband power spectrum) and the attractor is a fractal object with self-similarity [4,15,23]. The attractor associated with chaotic solutions are often termed as strange attractors as they do not fit any regular objects.

The minimum number of independent phase variables required to unambiguously define the state of the dynamical system is known as the dimension of the phase space for that particular system. For the case of a mathematical model of a dynamical system defined by differential equations, the number of first order ordinary differential equations describing the system gives us the dimension of the phase space. However, for the case of a physical system the number of independent state variables is not known a priori. Only time-series measurements of some physical quantity of the dynamical system which itself might be a combination of the inherent independent variables of the system are available. A phase space of the dynamical system can be reconstructed from this time series as per the embedding theorem [18]. The phase space reconstruction in this paper has been done using time-delay embedding method on both pressure and heat release rate time series data. However, before discussing the phase space reconstruction, we briefly discuss Poincaré sections which also play a major role in the analysis of dynamical systems.

3.2 Poincaré sections

A Poincaré section depicts the intersection of an orbit in the phase space with a plane called the Poincaré plane. Unlike the phase plots discussed above where we continuously follow the evolution of a system, in a Poincaré section we look at the state of the system only at discrete time intervals. Hence,

we get a set of points in the phase plane. Each classification of periodic and aperiodic motion has its own signature in the Poincaré section. To illustrate with examples, the Poincaré section of a simple limit cycle orbit will be a single point in a usual Poincaré section wherein the Poincaré plane is a semi-infinite plane, i.e., it extends only in one direction and two points in case of a two-sided Poincaré sections with an infinite plane. For periodic solutions with the presence of a $1/n$ subharmonic in the signal along with the dominant frequency (formally called a period n limit cycle), the two sided section will have $2n$ points. For quasi-periodic solutions, the two sided Poincaré section consists of bunch of points which fill up two closed curves. In contrast, for chaotic solutions, the points on the Poincaré section fill up regions in the phase space which are more than a curve and these regions also form a fractal structure. Poincaré sections obtained from the reconstructed phase portraits using pressure and heat release time series from the experiments will be presented in the following sections.

3.3 Phase Space Reconstruction using time-delay embedding

The embedding theorem [18] facilitates the construction of multivariate phase space from scalar observations. As is the case in experiments, discrete time series sampled at finite intervals of time of a particular variable from the system is available. According to the theorem, it is possible to unfold the geometric structure of the multivariate phase space of the system in a space created out of vectors obtained from the experimental time series. To elaborate, the scalar measurements $s(n) = s(t_o + n\tau_s)$, where τ_s is the sampling time can be used to create a vector in d dimensions :

$$\mathbf{y}(n) = [s(n), s(n+T), s(n+2T), \ldots, s(n+(d-1)T)], \tag{1}$$

where $s(n+T) = s(t_o + (n+T)\tau_s)$ are called time lagged variables. $T\tau_s$ is the time delay and d is the embedding dimension. This vector represents a point in the phase space. The collection of points obtained from the scalar measurements by taking $n = 0, 1, \ldots, N$ will give the phase portrait of the dynamical system.

Determination of time delay

Time delay used for the reconstruction should be large enough so that the various vectors in $\mathbf{y}(n)$ are independent to be able to capture the true dynamics of the system but not so large as to make the connection between the time lagged variables to become random due to numerical inaccuracies. Several methods are available in the literature to obtain the optimal time delay. The time delay for the current study is chosen as the first zero crossing of the autocorrelation function of the time series which is the optimal delay as suggested by [1, 2] and is found to be $T = 7$ as shown in Fig. 3(a).

Determination of embedding dimension

In order for the reconstructed phase space to capture the physical properties of an attractor with a dimension d_A, a sufficiently large dimension d should be chosen. The procedure of choosing a sufficiently large d is known as embedding and the minimum dimension that works for a time series is called the embedding dimension d_E [2] for that variable. Note that any $d \geq d_E$ will also provide an embedding. However, reconstructing the phase space of an attractor in a lower dimension than d_E is equivalent to projecting a higher dimensional structure onto a lower dimension. Again there are several methods available for identifying the embedding dimension from scalar measurements [16]. The 'false nearest neighbors' technique is one of these methods for determining the embedding dimension and is based on the fact that projection of a geometrical structure to a lower dimension space would lead to false crossings of the orbits within the structure. It is an iterative technique where the algorithm goes progressively from a small dimension to a higher dimension to check for any false orbit crossings until it finds a large enough dimension with no such crossings. Points that are brought close together in the reconstructed space due to these false crossings are termed as false nearest neighbors. The algorithm determines the fraction of false neighbors for each dimension starting from one until it reaches a stage where all the points in a dimension remain nearest neighbors even if the dimension is increased further [16]. A typically obtained graph for the variation of the percentage of false nearest neighbors against the embedding dimension obtained for a pressure time series data at $x_f = 33.9\ cm$, is shown in Fig.3. It is clear from this figure that the embedding dimension for our present case is $d_E = 4$. However for illustration of the phase portraits, we will only use a 3-dimensional phase space.

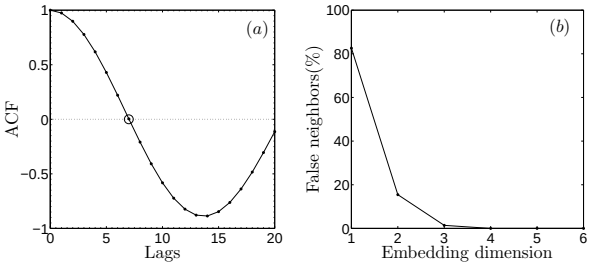

Figure 3: Calculation of time-delay (a) and embedding dimension (b) for phase space reconstruction of the phase portrait from pressure time series at $x_f = 33.9\ cm$.

Other concepts related to the nonlinear time-series analysis such as determination of the dimension of the attractor and the largest Lyapunov exponent which are useful for the characterization of chaotic motions are not discussed here due to lack of space even though they have been used in later discussions. Only the fundamental concept of the phase space reconstruction has been described briefly.

4 Results

As the flame location (x_f) was changed, it was observed that the system goes from a stable, non-oscillating state (region (I) in Fig.2) to an unstable, oscillating state. In the unstable regime, the system shows different types of oscillations which corresponds to the presence of different attractors. To identify the various attractors, time series data, power spectrum, phase plots and Poincaré sections are studied carefully. The analysis and corresponding results, are presented in the following subsections. It is to be noted that nonlinear filtering has been applied to the time series [19] for effective separation of the dynamics of the system from noise.

Limit cycle oscillations: Region II

The appearance of periodic oscillations from a steady state was observed at $x_f = 13.8\ cm$. There is a jump in the bifurcation diagram (Fig. 2) which can be seen at the emergence of the region marked (II). This jump is due to the subcritical nature of the Hopf bifurcation typical of thermoacoustic systems [13, 24]. Figure 4 which corresponds to $x_f = 13.8\ cm$, gives the time series of this state along with the power spectrum, 3D phase space plot and Poincaré sections. The regular sinusoidal time series for both the pressure and heat release rate oscillations indicate that the particular case is a limit cycle oscillation. Furthermore, the phase plot is a distinct closed loop, which is typical of these oscillations. The power spectrum plots show the presence of a single dominating frequency of 469 Hz along with its higher harmonics. The two sided Poincaré section at the plane $p(t+2\tau) = 0$ and $q(t+2\tau) = 0$ in Figs. 4d & 4h show two distinct points. As discussed earlier in the section on Poincaré section (section 3.2), this is a feature of limit cycle oscillations.

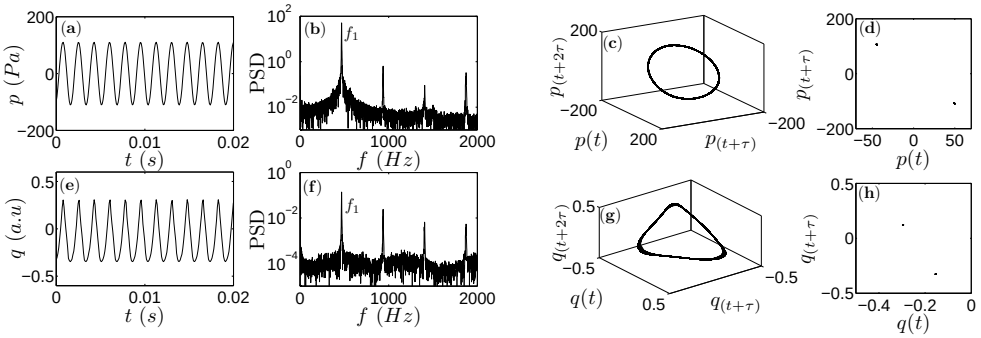

Figure 4: Limit cycle oscillations, $x_f = 13.8\ cm$: Region (II) in the bifurcation diagram (Fig. 2); (a-d) - time series, power spectrum , 3D phase plot and Poincaré section for pressure (p) oscillations; (e-h) - corresponding plots for heat release rate (q) oscillations; $f_1 = 469 Hz$.

On changing the flame location further, the features of the oscillations start exhibiting interesting changes. The time series data shows that the oscillations become more complicated than the limit cycle oscillations that were observed in region (II).

Quasi-periodic oscillations: Region III

Referring back to the bifurcation diagram (Fig. 2), a change is observed in the oscillations again at $x_f = 16\ cm$. As is evident from Fig. 5, the behavior of the oscillations changes to a quasi-periodic state. The power spectrum (Figs. 5b & 5f) show the presence of more than one characteristic frequencies. This is reflected in the time series data and phase plots for both p and q oscillations. The major peaks in the power spectrum occur at frequencies - f_1, f_2 and f_3 along with other minor peaks, where $f_1 = 469\ Hz$, $f_2 = 303\ Hz$ are the characteristic frequencies and $f_3 = 166\ Hz = f_1 - f_2$. Note that the characteristic frequencies are incommensurate to each other and as a result, the obtained phase trajectory in the quasi-periodic motion never returns to the same point. Instead it evolves on the surface of a torus. The presence of a toroidal structure of the phase portrait (Figs. 5c & 5g) confirms the presence of quasi-periodic oscillations. Also the Poincaré sections (Figs. 5d & 5h) clearly show the points filling out distinct curves on the Poincaré plane which indicates a quasi-periodic solution. The quasi-periodic solution appears as a result of a Hopf bifurcation of the limit cycle,which is formally known as a Neimark-Sacker bifurcation [16]. The system stays in this state till the flame location $x_f = 19\ cm$, at which point, the torus becomes unstable and breaks down into a structure (strange attractor) shown in Fig. 6. This transition is indicated in the bifurcation diagram (Fig. 2) as region (IV). Oscillations in Region (IV) are mostly chaotic and were observed to display a variety of other states with remarkably different features hinting towards the possible routes to chaos.

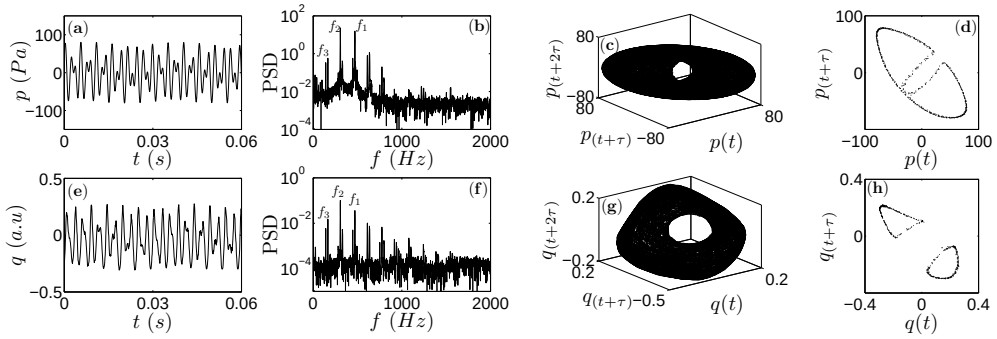

Figure 5: Onset of quasi-periodic behavior, $x_f = 16.2\ cm$: Region (III) in the bifurcation diagram (Fig. 2); (a-d) - time series, power spectrum, 3D phase plot and Poincaré section for pressure (p) and heat release rate oscillations; - corresponding plots for heat release rate (q) oscillations; $f_1 = 469\ Hz$, $f_2 = 303\ Hz$, $f_3 = 166\ Hz$.

Chaotic: Region IV

At the onset of region (IV), a strange attractor [16,23] emerges out of the toroidal structure of a quasi-periodic state in Region (III). A chaotic orbit forms a strange attractor when it moves about in the phase space in an unpredictable almost random like motion. A strange attractor may be classified by its fractal dimension [15] since it is a fractal object and has a non-integer dimension. Correlation dimension [6,15] is one of the measures to identify the fractal dimension of an attractor. The correlation dimension calculated for the attractor observed at $x_f = 19.2\ cm$ (Fig. 6.) in region (IV) is 2.85 which is an indication that it is a strange attractor. The irregularity in the oscillations can be clearly seen in the pressure and heat release rate time series in Figs. 6a & 6e. In the Poincaré section, the intersections of the strange attractor orbit with the plane shows scattered points as is seen in Figs. 6d & 6h. The power spectrum (Figs. 6b & 6f) shows the presence of numerous peaks around the characteristic frequencies of the oscillations obtained earlier with a distinct third characteristic frequency around 646 Hz. The broad band nature of the power spectrum further suggests the presence of a chaotic state. The appearance of a third characteristic frequency suggests that the 2-D torus breaks down into a strange attractor through the formation of an unstable 3-D torus. Accordingly the route to chaos is the Ruelle-Takens quasi-periodic route [7].

The trajectories on the strange attractor move in the phase space randomly, unable to follow a periodic orbit. However with a change in the bifurcation parameters, the frequencies also change and they

might get related rationally. In such a case, the trajectories become regular (almost periodic) resulting in a frequency-locked state. Frequency-locking was observed in our system within region (IV) at the flame location $x_f = 21\ cm$. Figure 7 shows this case of frequency-locking when the chaotic state is locked in an almost periodic motion on a torus (Figs. 7c & 7g). The power spectrum gets filled with distinct peaks which are harmonics of the characteristic frequencies (Figs. 7b & 7f). Reconstruction using the pressure signal (Fig. 7c) shows a periodic motion about a torus which becomes more evident from the Poincaré as shown in section in Fig. 7d with only finitely many points. However the phase space reconstruction using the heat release rate data (q) (Fig. 7g) clearly indicates that the solution is not purely periodic but has some finite width. Hence, the system evolves to a chaotic state from a quasi-periodic behavior and then goes to an intermediate frequency-locked state before getting back to chaotic behavior. As the flame location is changed further, the system switches to another frequency-locked state which persists for a long range of x_f (region (V) of the bifurcation diagram, Fig. 2).

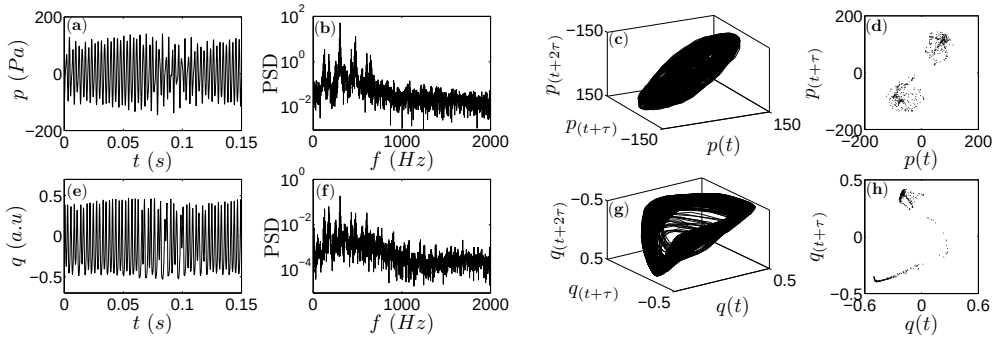

Figure 6: Chaotic state, $x_f = 19.2\ cm$: Region (IV) in the bifurcation diagram (Fig. 2); (a-d) - time series, power spectrum, 3D phase plot and Poincaré section for pressure (p) oscillations; (e-h) - corresponding plots for heat release rate (q) oscillations.

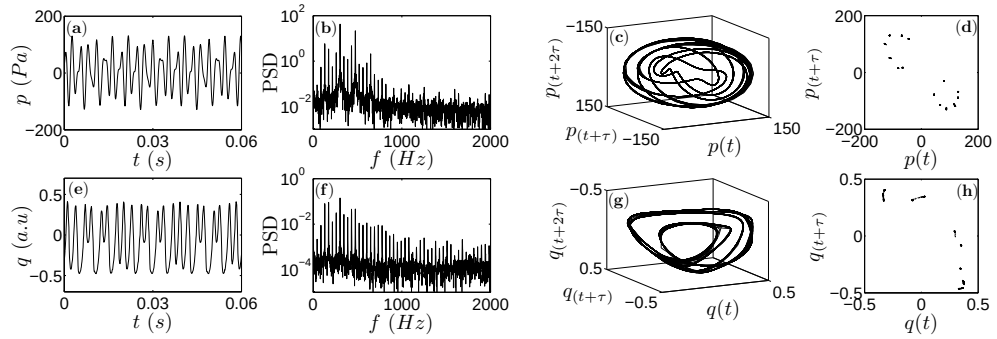

Figure 7: Frequency-locking, $x_f = 21\ cm$: Region (IV) in the bifurcation diagram (Fig. 2); (a-d) - time series, power spectrum , 3D phase plot and Poincaré section for pressure (p) oscillations; (e-h) - corresponding plots for heat release rate (q) oscillations.

Frequency-locked and Chaotic states followed by quasi-periodic state: Region V and VI

As the bifurcation parameter (x_f) enters region (V) it was observed that the oscillations become regular again (Figs. 8a & 8e) at x_f of 25.8 cm. These oscillations have strong signature of period- 4 motions since the power spectrum of the pressure signal (Fig. 8b) shows frequency peaks at f_1, $f_1/2$ and $f_1/4$ with $f_1 = 304\ Hz$. The dominating frequency of the system has changed from 469 Hz to 304 Hz. The phase portrait reconstructed from pressure signal and heat release rate time series(Figs. 8c & 8g) shows a limit cycle behavior with two loops as the contribution from subharmonic $f_1/4$ is significantly less. The

Poincaré section (Fig. 8h) also shows that the dynamics is more complicated than a period-4 oscillation and this region basically corresponds to a frequency-locked state.

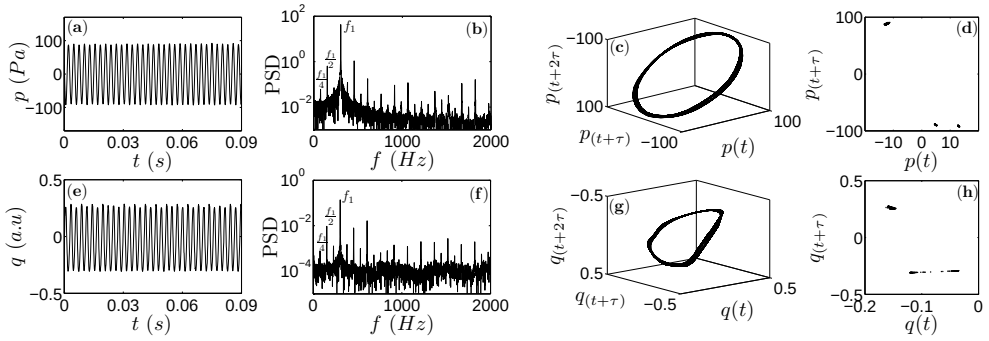

Figure 8: Period-4 oscillations, $x_f = 25.8\ cm$: Region (V) in the bifurcation diagram (Fig. 2); $f_1 = 305\ Hz$; (a-d) - time series, power spectrum , 3D phase plot and Poincaré section for pressure (p) oscillations; (e-h) - corresponding plots for heat release rate (q) oscillations.

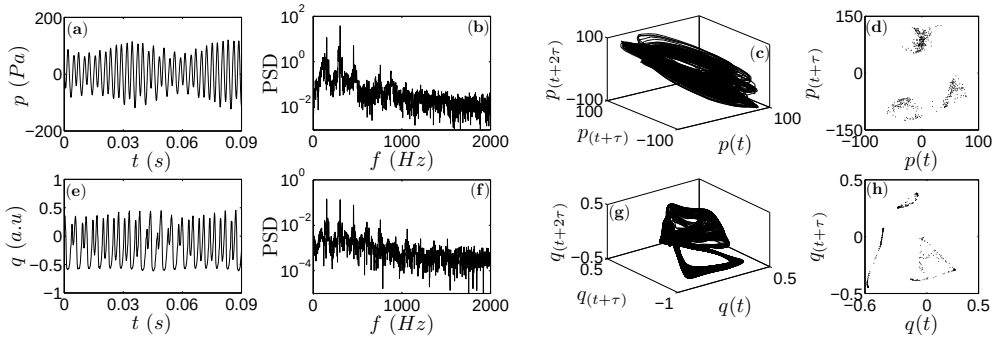

Figure 9: Chaotic state (correlation dimension = 2.39), $x_f = 33.9\ cm$: Region (VI) in the bifurcation diagram (Fig. 2); (a-d) - time series, power spectrum , 3D phase plot and Poincaré section for pressure (p) oscillations; (e-h) - corresponding plots for heat release rate (q) oscillations.

This state of the system existed till the flame location x_f of 33.8 cm. Region (VI) that follows this region is again a region of chaotic oscillations with narrow windows of frequency-locked states similar to the results obtained for region (IV). Similar chaotic behavior were also observed in this region. Figure 9 corresponds to time series data obtained for $x_f = 33.9\ cm$, and it clearly shows the characteristics of the chaotic behavior observed in region (VI). The power spectrum distinctly shows three broadband regions centered around 304 Hz, 152 Hz and 457 Hz where the frequency 152 Hz is just half of 304 Hz. The presence of only two characteristic frequencies in this chaotic state suggest that chaos is generated in this regime not by the appearance of a third frequency but through the frequency-locking quasi-periodic route [7]. This route is also suggested by the presence of a number of windows of frequency-locked states between two chaotic states. In fact with an increase in the flame location the system gradually moves from a chaotic behavior to a regular behavior with the broadband of the power spectrum narrowing down to distinct peaks. There is a very narrow window of quasi-periodic solutions before the solutions enter region (VII) of period-2 oscillations. Such a quasi-periodic response is demonstrated in Fig. 10 for $x_f = 40\ cm$.

Period two oscillations: Region VII

As the flame location was moved further, the oscillations entered the state given by region (VII) in the bifurcation plot (Fig. 2). In the bifurcation plot itself, we find each flame location has two amplitudes

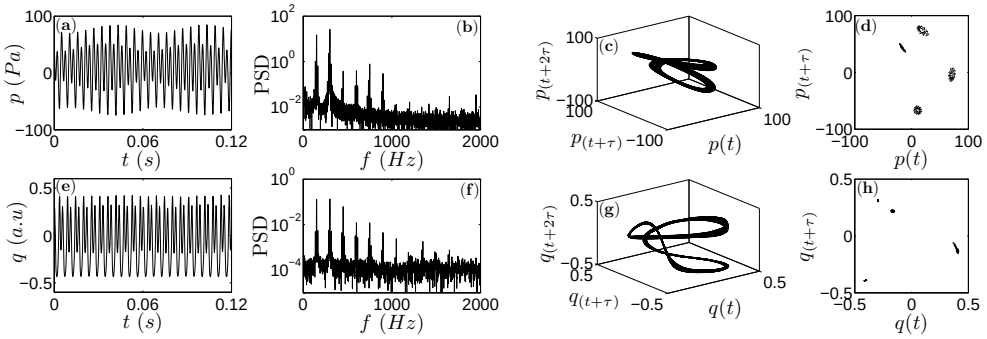

Figure 10: Quasi-periodic behavior, $x_f = 40cm$: Region (VI) in the bifurcation diagram (Fig. 2); (a-d) - time series, power spectrum , 3D phase plot and Poincaré section for pressure (p) oscillations; (e-h) - corresponding plots for heat release rate (q) oscillations.

representing the oscillations. This is typical of a period-2 oscillation. In Fig. 11, we find the characteristics of this particular variety of oscillation in the thermoacoustic system. The power spectrum has peaks at f_1 and $f_1/2$ with $f_1 = 300\ Hz$. The phase plot shows an orbit forming two loops indicating a doubling of time period of the oscillations when compared to the situation of limit cycle oscillations where we had a single loop in the phase space. Figures 11d and 11h show the two sided Poincaré section for this case of period-2 oscillations. Beyond this point, period-2 oscillations existed in the system till the flame location of 43.9 cm after which the system returned to a steady non-oscillating state.

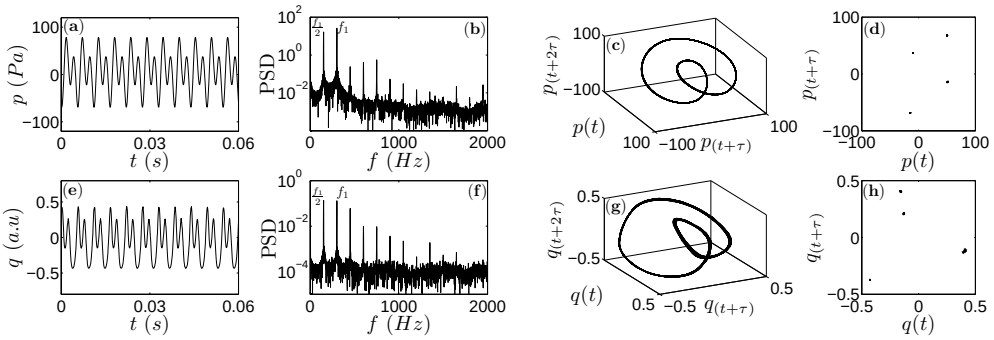

Figure 11: Period-2 oscillations, $x_f = 41.7\ cm$: Region (VII) in the bifurcation diagram (Fig. 2); (a-d) - time series, power spectrum , 3D phase plot and Poincaré section for pressure (p) oscillations; (e-h) - corresponding plots for heat release rate (q) oscillations; $f_1 = 300\ Hz$.

Discussion

According to the dynamical systems theory, there are various possible routes to chaos [4, 7]. For our system reported in this paper, we have found that the first unsteady solution from the steady state appears in the form of a limit cycle which subsequently becomes chaotic through the quasi-periodic route to chaos. On calculation of the Lyapunov exponent of the chaotic solution given in Fig. 9, using the algorithm given by Kantz [9], we get the maximal Lyapunov exponent as 0.23 which confirms that the state is chaotic in nature. Both the Ruelle-Takens route as well as the frequency-locking route have been obtained in our experiments. There is another transition from the unsteady state to the steady state at the flame location $x_f = 43.9\ cm$. Here the involved unsteady state is a period-2 limit cycle instead of a simple limit cycle. Dynamical systems theory describes a limit cycle arising from a Hopf bifurcation. However, as mentioned earlier, this bifurcation is subcritical in nature as a result of which the resulting limit cycles could be unstable and the first stable unsteady solutions observed in experiments could be a period-2 or quasi-periodic solution which are generated from the limit cycles through secondary bifurcations. In fact, many of the other cases where different equivalence ratios and air flow rates were

chosen, started with either a period-2 or a quasi-periodic state as the transition from non-oscillating to the self excited state. The rest of the process followed the same behavior as is followed by the present configuration. The whole sequence of major states observed in the present study can be summarized as follows:

$$Steady(S) \rightarrow Periodic(P) \xrightarrow{Neimark-Sacker\,(NS)} Quasi-periodic(QP) \xrightarrow{Ruelle-Takens}$$

$$Chaotic \xrightarrow{Frequency-locking} P(period-4) \rightarrow Chaotic \xrightarrow{Frequency-locking} QP \xrightarrow{NS} P(period-2) \rightarrow S$$

The strange attractors observed in our system are an indication of the presence of chaotic solutions in the system. The presence of chaos alters the spectral content of the oscillations. This information may be important for the structural design of components. Chaotic oscillations in thermoacoustic systems have been reported earlier in literature. Fichera [5], in his study on a lean premixed gas turbine combustor, reported the presence of chaotic oscillations through topological (phase space) analysis and confirmed its existence by calculating attractor dimension and Lyapunov exponents for the obtained data. Lei and Turan [12] observed the existence of multiple solutions along with chaos in his theoretical study that involved modal analysis of thermoacoustic instability. However, the gradual change in system dynamics with change in the control parameter has not been explored in detail and hence the route to chaos could not be established. The primary aim of the current work is to study the changes in the system dynamics and understand the routes to chaos in our thermoacoustic system. Our system is shown to possess a diverse variety of nonlinear behavior. This richness can be ascribed to the nonlinearity of the thermoacoustic phenomenon.

5 Conclusions

In this paper, the nonlinear nature of thermoacoustic oscillations has been investigated in the light of the dynamical systems theory. This approach enabled us to characterize and classify the behavior of the system in the linearly unstable regime. A variety of attractors - periodic, quasi-periodic and chaotic states, were observed in the system as a control parameter was changed. Similar behavioral patterns in the oscillations have been observed to occur in several other nonlinear processes occurring in nature. The phenomena observed in this study are related to the inherent nonlinear processes in thermoacoustic instability. Hence, this information is quite critical in constructing accurate models for thermoacoustic instability and designing effective control techniques.

6 Acknowledgments

This work was funded by the Department of Science and Technology. The authors would like to acknowledge Dr. S. Ducruix (Ecole Centrale), Dr. S.R. Chakravarthy (IIT Madras) and Dr. T.M. Muruganandam (IIT Madras) for their critical suggestions and comments on the design of the setup. We also thank Dr. V. Balakrishnan (IIT Madras), Dr. Neelima Gupte (IIT Madras), Dr. Sunetra Sarkar (IIT Madras) and Dr. M.K. Verma (IIT Kanpur) for the discussions on the theory of nonlinear dynamics.

References

[1] H. D. I. Abarbanel. *Analysis of Observed Chaotic Data.* Springer-Verlag New York, Inc., 1996.

[2] H. D. I. Abarbanel, R. Brown, J. J. Sidorowich, and L. S. Tsimring. The analysis of observed chaotic data in physical systems. *Rev. Mod. Phys.*, 65(4):1331–1392, 1993.

[3] A. P. Dowling and S. R. Stow. Acoustic analysis of gas turbine combustors. *Journal of Propulsion and Power*, 19(5):751–763, 2003.

[4] P. G. Drazin. *Nonlinear Systems.* Cambridge University Press, 1992.

[5] A. Fichera, C. Losenno, and A. Pagano. Experimental analysis of thermo-acoustic combustion instability. *Applied Energy*, 70(2):179 – 191, 2001.

[6] P. Grassberger and I. Procaccia. Characterization of strange attractors. *Phys. Rev. Lett.*, 50(5):346–349, Jan 1983.

[7] R. C. Hilborn. *Chaos and Nonlinear Dynamics: An Introduction for Scientists and Engineers*. Oxford University Press, 2000.

[8] C. C. Jahnke and F. E. C. Culick. Application of dynamical systems theory to nonlinear combustion instabilities. *Journal of Propulsion and Power*, 10(4):508–517, 1994.

[9] H. Kantz. A robust method to estimate the maximal Lyapunov exponent of a time series. *Physics Letters A*, 185(1):77 – 87, 1994.

[10] N. Karimi, M. J. Brear, and S.H. Jin. Nonlinear dynamics of thermoacoustic instability using a kinematic, premixed flame model. *15th Australasian fluid Mechanics Conference, The University of Sydney, Sydney, Australia*, 2004.

[11] S. Lei and A.Turan. Nonlinear/chaotic analysis modelling and control of combustion instabilities due to vaporizing sprays. *Chaos, Solitons & Fractals*, 42(3):1766–1779, 2009.

[12] S. Lei and A. Turan. Nonlinear/chaotic behaviour in thermo-acoustic instability. *Combustion Theory and Modelling*, 13(3):541–557, 2009.

[13] T. C. Lieuwen. Experimental investigation of limit-cycle oscillations in an unstable gas turbine combustor. *Journal of Propulsion and Power*, 18(1):61–67, 2002.

[14] T. C. Lieuwen and V. Yang. *Combustion Instabilities in Gas Turbines - Operational Experience, Fundamental Mechanisms, and Modelling*, volume 210. Progress in Astronautics and Aeronautics, American Institute of Aeronautics and Astronautics, Inc, 2005.

[15] F. C. Moon. *Chaotic and Fractal Dynamics: An Introduction for Applied Scientists and Engineers*. Wiley-VCH Verlag GmbH & Co. KGaA, Weinheim, 2004.

[16] A. H. Nayfeh and B. Balachandran. *Applied Nonlinear Dynamics: Analytical, Computational, and Experimental Methods*. Wiley-VCH Verlag GmbH & Co. KGaA, Weinheim, 2004.

[17] N. Noiray, D. Durox, T. Schuller, and S. Candel. A unified framework for nonlinear combustion instability analysis based on the flame describing function. *Journal of Fluid Mech*, 615:139–167, 2008.

[18] D. Ruelle and F. Takens. On the nature of turbulence. *Communication in Mathematical Physics*, 20(3):167–192, 1971.

[19] T. Schreiber. Extremely simple nonlinear noise-reduction method. *Phys. Rev. E*, 47(4):2401–2404, Apr 1993.

[20] T. Schuller, D. Durox, and S. Candel. A unified model for the prediction of laminar flame transfer functions: comparisons between conical and V-flame dynamics. *Combustion and Flame*, 134(1-2):21 – 34, 2003.

[21] J. D. Sterling and E. E. Zukoski. Nonlinear dynamics of laboratory combustor pressure oscillations. *Combustion Science and Technology*, 77:225–238, 1991.

[22] J.D. Sterling. Nonlinear analysis and modelling of combustion instabilities in a laboratory combustor. *Combustion Science and Technology*, 89:167–179, 1993.

[23] S. H. Strogatz. *Nonlinear Dynamics And Chaos: With Applications To Physics, Biology, Chemistry, And Engineering (Studies in nonlinearity)*. Levant Books, 2007.

[24] P. Subramanian, S. Mariappan, R.I Sujith, and P. Wahi. Application of numerical continuation to bifurcation analysis of Rijke tube. *Summer School and Workshop on Nonnormal and Nonlinear Effects in Aero and Thermoacoustics, May 17th-21st, Munich*, 2010.